

Solar-Driven Reduction of 1 atm CO₂ to Formate at 10% Energy-Conversion Efficiency by Use of a TiO₂-Protected III-V Tandem Photoanode in Conjunction with a Bipolar Membrane and a Pd/C Cathode Electrocatalyst

Xinghao Zhou^a, Rui Liu^b, Ke Sun^b, Yikai Chen^b, Erik Verlage^a, Sonja A. Francis^b, Nathan S Lewis^b and ChengXiang Xiang^b

^a Division of Engineering and Applied Science, Department of Applied Physics and Materials Science, California Institute of Technology, Pasadena, CA, 91125, USA

^b Division of Chemistry and Chemical Engineering, California Institute of Technology, Pasadena, CA, 91125, USA

A solar-driven CO₂-reduction (CO₂R) cell, consisting of a tandem GaAs/InGaP/TiO₂/Ni photoanode in 1.0 M KOH(aq) (pH=13.7) to facilitate the oxygen-evolution reaction (OER), a Pd/C nanoparticle-coated Ti mesh cathode in 2.8 M KHCO₃(aq) (pH=8.0) to perform the CO₂R reaction, and a bipolar membrane to allow for steady-state operation of the catholyte and anolyte at different bulk pH values, was constructed. At the operational current density of 8.5 mA cm⁻², in 2.8 M KHCO₃(aq), the cathode exhibited <100 mV overpotential and >94% Faradaic efficiency for the reduction of 1 atm of CO₂(g) to formate. The anode exhibited 320 ± 7 mV overpotential for the OER in 1.0 M KOH(aq), and the bipolar membrane exhibited ~480 mV voltage loss with minimal product crossover as well as >90% and >95% selectivity for protons and hydroxide ions, respectively. The solar-driven CO₂R cell converted sunlight to fuels at an energy-conversion efficiency of ~10%.

Introduction

The sustainable electrochemical reduction of CO₂ to fuels requires utilization of CO₂ from the atmosphere as well as use of the electrons and protons produced by the oxidation of water to O₂(g)(1, 2). However, the optimal electrolyte for CO₂ reduction (CO₂R) is quite different than that for the oxidation of water. For CO₂R, the low concentration of dissolved CO₂ under alkaline conditions (e.g., pH>10) imposes severe mass-transport limitations on the electroactive reagent(3-5), whereas under acidic conditions (e.g., pH<1), the high proton concentration favors the competing hydrogen-evolution reaction (HER). Hence, the development of catalysts for CO₂R has generally focused on electrolytes having near-neutral pH values(6, 7). At present, in near-neutral pH electrolytes, only electrochemical processes that involve the two-electron/two-proton reduction of CO₂, to produce either CO or formate, can be performed efficiently and selectively at an operating current density of 10¹ mA cm⁻²(6, 8-11). In contrast, for the oxygen-evolution reaction (OER), mixed-metal oxides have been extensively studied in strongly alkaline conditions (1.0 M KOH(aq)), with state-of-the-art catalysts exhibiting ~250 – 300 mV overpotentials at 10 mA cm⁻² of anodic current density(12, 13).

Electrocatalysts for the OER in near-neutral electrolytes exhibit substantially larger overpotentials than OER electrocatalysts in strongly alkaline electrolytes(13-15), because the negatively charged hydroxide ion is more readily oxidized than a neutral water molecule, and hydroxide is present in high concentration in alkaline solutions(16).

This work is a summary of the previously published demonstration of a solar-driven CO₂R with 10% energy-conversion efficiency(17). We used a bipolar membrane to facilitate effective coupling between two electrodes and electrolytes, one for CO₂R and one for the OER, that typically operate at mutually different pH values, and to produce a lower total cell overvoltage than known single-electrolyte CO₂R systems.

Experimental

The preparation of electrodes comprising Pd/C on a Ti mesh was similar to that reported previously for Pd/C on a Ti foil electrode(8). A Ti mesh was first cut into 0.04 cm² pieces. Five pieces of Ti mesh were stacked and stringed together with a Ti wire. The stacked Ti mesh was etched in boiling 10% oxalic acid, rinsed thoroughly with H₂O, and dried overnight at 75 °C in an oven. 4.8 mg of Pd/C powder was then mixed with 2.4 ml isopropanol and 40 μL 10 wt.% Nafion and the mixture was sonicated for > 30 min. The resulting solution was drop-casted onto the Ti mesh, with a Pd mass loading of 250 μg cm⁻². The Pd mass loading of Pd/C coated Ti foil reported previously was 50 μg cm⁻². As a comparison, a Pd/C nanoparticle-coated Ti foil electrode was made using the same conditions as on the Ti mesh except that the Pd mass loading was 50 μg cm⁻². The preparation of GaAs/InGaP/TiO₂/Ni photoanode was the same as those previous reported(18, 19).

The two-electrode electrochemical setup is shown in Figure 1. Two custom-made three-necked cells were used in the 3-electrode measurement. The BPM was used for prevention of crossover of the formate product, and to prevent the formate from being oxidized at the counter electrode. The electrolyte was vigorously agitated with a magnetic stir bar driven by a model-train motor (Pittman) with a Railpower 1370 speed controller (Model Rectifier Corporation). CO₂(g) was bubbled into the KHCO₃ solution during electrochemical measurements, to prevent oxygen dissolution. A peristaltic pumping system (Simply Pumps PM300F) with a minimum flow rate of 500 mL min⁻¹, as controlled by a tunable power supply, was used to facilitate the removal of CO₂ bubbles at the BPM surface, and to minimize the voltage loss at the BPM caused by bubbles. A Xe arc lamp (Newport 67005 and 69911) equipped with an IR filter (Newport 61945) and with an AM 1.5 filter (Newport 81094 and 71260) was used as the light source for *J-E* measurements. The intensity in the solution-containing cell was then calibrated by placing a Si photodiode (FDS100-Cal, Thorlabs) with a similar area as that of the photoanode (0.03 cm²) in the custom-made three-necked beaker with flat quartz windows, with the Si located at nominally the same position as that occupied by the exposed area of the photoelectrode. The Si photodiode had been previously calibrated by measurement of the short-circuit current density under 100 mW cm⁻² of AM 1.5 simulated sunlight. The area of the anode, membrane and Pd/C cathode were 0.03 cm², 0.03 cm², 0.04 cm², respectively. A 0.2 cm diameter hole was punched at the middle of a piece of rubber using a hole making tool. An O-ring with 0.2 cm diameter was glued with epoxy on the rubber with the hole aligned. The BPM was right between two pieces of rubber, and the

hard rubber/O-ring/BPM/O-ring/hard rubber assembly was tightly clamped between the two cells as shown in Figure 1.

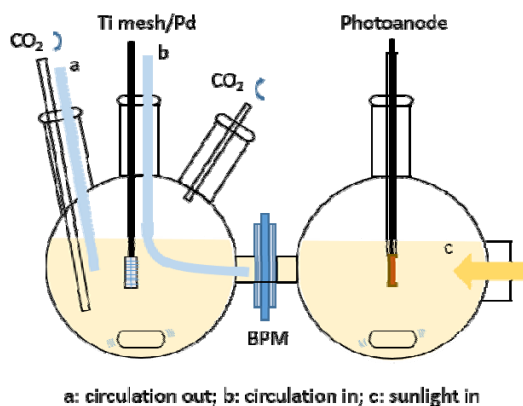


Figure 1. Schematic illustration of a two-electrode electrochemical setup. The anolyte is 1.0 M KOH(aq), and the catholyte is 2.8 M KHCO₃(aq). (Reprinted with permission from Ref. (17) Copyright 2016 American Chemical Society.)

Results and Discussion

Cathode half cell

The Pd/C-coated stacked Ti mesh electrode (red curve in Figure 2A) exhibited improved performance compared to the Pd/C-coated Ti foil (black curve in Figure 2A), because of the increased mass loading and larger electrochemically accessible surface area for CO₂R reduction. The forward scan indicated that the onset potential of cathodic current was close the equilibrium potential for CO₂ reduction to formate ($E^{\circ}(\text{CO}_2/\text{HCOO}^-) = -0.687 \text{ V}$ versus the Ag/AgCl reference electrode)(20). An overpotential of $-57 \pm 8 \text{ mV}$ was required to drive the CO₂R reaction at a cathodic geometric current density of 10 mA cm^{-2} .

Figure 2B shows the Faradaic efficiency for the production of formate using the Pd/C nanoparticle-coated Ti mesh cathode in CO₂-saturated 2.8 M KHCO₃(aq) as a function of time, at four different overpotentials. At all overpotentials, near-unity Faradaic efficiency was observed for the first 60 min of operation. The Faradaic efficiency then decreased slowly for overpotentials between -45 mV and -120 mV , but still exceeded $\geq 94\%$ after 3 h of electrolysis (Figure 2B). In contrast, when the electrode was held at -170 mV vs $E^{\circ}(\text{CO}_2/\text{HCOO}^-)$, the Faradaic efficiency decayed quickly after 90 min, and decreased to $\sim 80\%$ after 3 h of continuous operation. The decrease of the Faradaic efficiency for formate production is consistent with the accumulation of CO at the surface of the Pd nanoparticles(8).

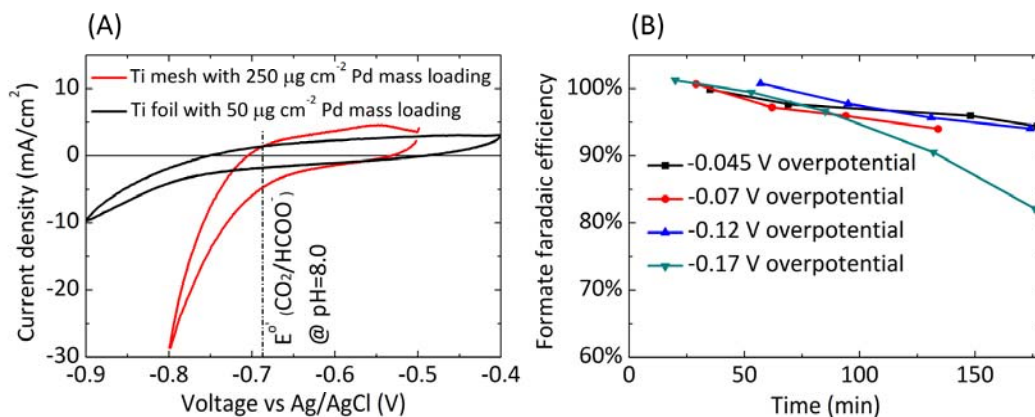


Figure 2. (A) Cyclic voltammetry of the Pd/C nanoparticle-coated stacked Ti mesh electrode with a Pd mass loading of 250 $\mu\text{g cm}^{-2}$ (red) and the Pd/C nanoparticle-coated Ti foil with a Pd mass loading of 50 $\mu\text{g cm}^{-2}$ (black) in CO₂-saturated 2.8 M KHCO₃(aq) at pH=8.0. The dotted line indicates the equilibrium potential for CO₂ reduction to formate at pH=8.0. (B) Faradaic efficiency of formate production as a function of time, for four different overpotentials, using the Pd/C nanoparticle-coated Ti mesh in CO₂-saturated 2.8 M KHCO₃(aq).

Anode half cell

To characterize in detail the performance of the protection layer and electrocatalytic components of the anode, Figure 3 shows the current density vs potential (J - E) behavior of a p⁺-Si/TiO₂/Ni dark anode effecting the OER in 1.0 M KOH(aq) (black) and in 2.8 M KHCO₃(aq) (red), respectively, without any correction for uncompensated resistance. The J - E behavior of p⁺-Si/TiO₂/Ni dark electrode was used to provide a measure of the overpotentials of the OER catalyst in 1.0 M KOH(aq) and in 2.8 M KHCO₃(aq). As shown in Figure 3, an overpotential of 330 ± 10 mV was required to produce a current density of 10 mA cm⁻² in 1.0 M KOH(aq), consistent with previous results(21). In contrast, an overpotential of 793 ± 26 mV was required in 2.8 M KHCO₃(aq) to produce 10 mA cm⁻² of current density.

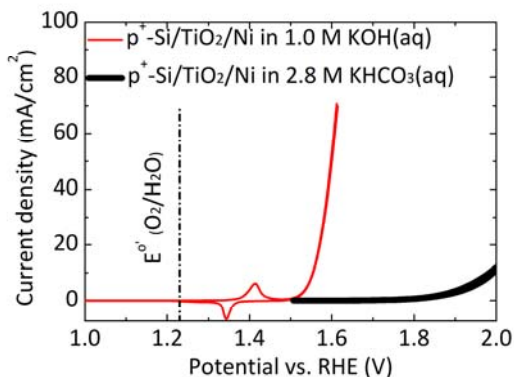


Figure 3. Current-voltage behavior of a p⁺-Si/TiO₂/Ni electrode for the oxygen-evolution reaction (OER) in 1.0 M KOH(aq) (red) and in 2.8 M KHCO₃(aq) (black).

Bipolar membrane properties

With the anolyte at pH = 13.7 (1.0 M KOH(aq)) and the catholyte at pH = 8.0 (2.8 M KHCO₃(aq)), Figure 4A shows membrane voltage loss (left axis), as well as measured

total membrane voltage (right axis) as a function of the current density normalized to the bipolar membrane (BPM) area. Two Luggin capillaries with Ag/AgCl reference electrodes were used to measure the electric potential drop across the bipolar membrane. The equilibrium potential, $V_{\text{membrane, equilibrium}}$ was calculated to be 0.336 V in the anolyte/catholyte system. At a current density of 10 mA cm⁻², the measured membrane total voltage was 0.843 ± 0.038 V. Hence, to drive the CO₂ reduction to formate at steady state, the voltage loss in the BPM, $V_{\text{membrane, loss}} = V_{\text{membrane, total}} - V_{\text{membrane, equilibrium}} = 0.843 \text{ V} - 0.059 \text{ V} \times (13.7 - 8.0)$, was 0.507 V. The voltage loss primarily resulted from the resistance loss of the bipolar membrane as well as from the overvoltage required for water dissociation at the transition region in the bipolar membrane. To evaluate the ionic transport properties of the membrane, a cell with Pt mesh electrodes as the cathode and anode was operated continuously for 100 h at a current density of ~8.5 mA cm⁻² normalized to the bipolar membrane area, with a resulting change by ~0.01 unit in the pH of the anolyte. If 100% of the charge passed were used for electro dialysis of the electrolytes, the pH of the anolyte would have changed by > 1 unit. Alternatively, for operation of CO₂R and OER in the same electrolyte, a cation exchange membrane, e.g., Nafion, could be used to separate the cathode chamber from the anode chamber. Figure 4B shows the measured total membrane voltage as a function of the current density normalized to the Nafion area, when both the anolyte and catholyte were 2.8 M KHCO₃(aq), but Nafion was used instead of a bipolar membrane. The total Nafion membrane voltage was equal to the Nafion membrane voltage loss, which largely arose due to the membrane resistance for transport of K⁺ ions. At a current density of 10 mA cm⁻², the Nafion membrane voltage loss was 214 ± 15 mV.

The ion-crossover fluxes in the BPM system were characterized using inductively coupled plasma mass spectrometry (ICPMS) in conjunction with a total inorganic carbon (TIC) analyser, to measure the ion concentrations in the catholyte and anolyte after charge was passed through the BPM at different current densities. At two different operational current densities, Figures 4C and 4D show the time-dependence of the selectivity for protons and hydroxide ions, respectively, through the bipolar membrane. Two major crossover pathways under the electric field, cation crossover from the anolyte to the catholyte, and anion crossover from the catholyte to the anolyte, were present due to the imperfect permselectivity of the cation-exchange membrane and anion-exchange membrane portions of the BPM. To determine the cation crossover, the KHCO₃(aq) catholyte was replaced by CsHCO₃(aq), so that small increases in the K⁺ concentration could be detected. The measured K⁺ leak rate in the CsHCO₃(aq)/KOH(aq) configuration also presented an upper bound for the behavior of the KHCO₃(aq)/KOH(aq) configuration due to the absence of the diffusional driving force for K⁺ transport from the anolyte to the catholyte in the all-K⁺-containing system. The membrane selectivities, f_{H^+} (f_{OH^-}), were defined as the ratio of proton-carried (hydroxide-carried) charge passed relative to the total charge passed through the membrane. At an operational current density of 3 mA cm⁻², the potassium leak current and the bicarbonate leak current constituted 10 - 25% and 20 - 35%, respectively, of the total current passed through the bipolar membrane. When the membrane current density was increased to 8 mA cm⁻², the membrane selectivity for protons increased to >90%, and the membrane selectivity for hydroxide ions increased to >95%. The crossover of the formate product was low (Figure 5). In the 3-electrode electrochemical measurement, the cathode compartment was separated by from the Pt counter electrode by a BPM, so the high Faradaic efficiency (>94%) measured in the cathode compartment at low overpotentials (from -45 mV to -120 mV, Figure 1B) also provides evidence for a low rate of formate crossover

through the BPM. The product crossovers were minimal because the negatively charged formate ion was effectively blocked by the negatively charged cation-exchange membrane in the bipolar membrane system.

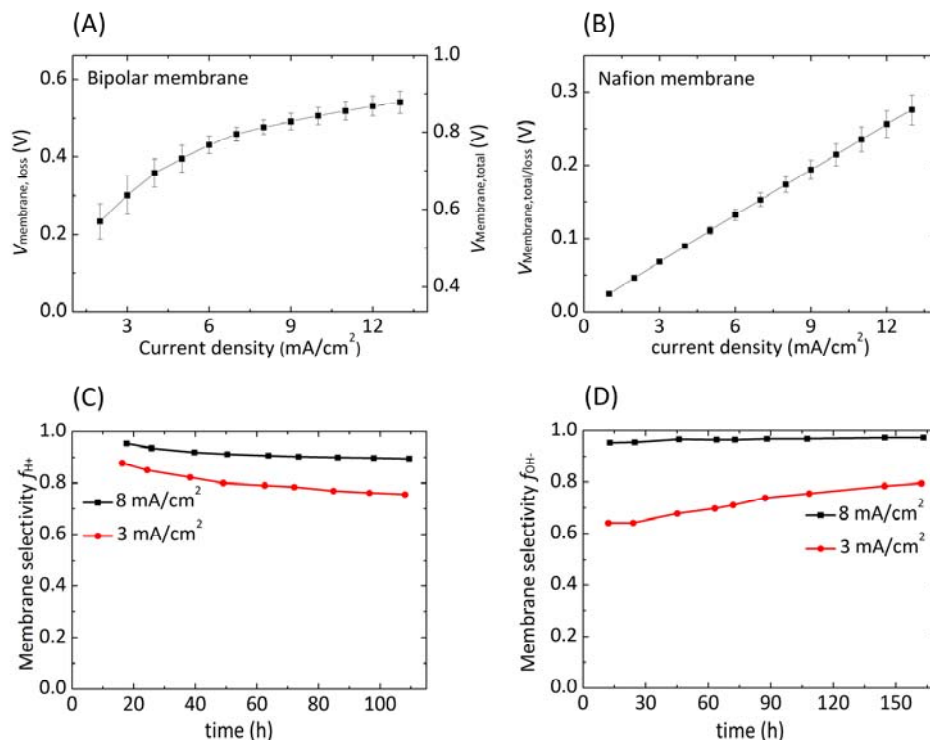


Figure 4. (A) Membrane voltage loss (left axis) and measured total membrane voltage (right axis) as a function of the current density normalized to the 0.03 cm^2 BPM area. The cell configuration was $\text{KHCO}_3(\text{aq})$ (pH=8.0)/BPM/ $\text{KOH}(\text{aq})$ (pH=13.7). (B) Measured total membrane voltage (or membrane voltage loss) as a function of the current density normalized to the Nafion area. The cell configuration was $\text{KHCO}_3(\text{aq})$ (pH=8.0)/Nafion/ $\text{KHCO}_3(\text{aq})$ (pH=8.0) (C) Selectivity of the bipolar membrane for protons as a function of time, when operated at two different current densities. (D) Selectivity of the bipolar membrane for hydroxide ions as a function of time, for two different current densities. Pt mesh electrodes were used as cathode and anode in (A-D).

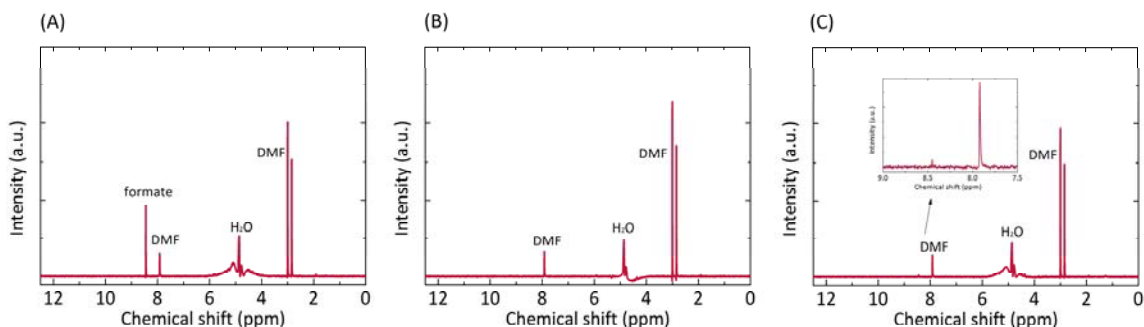


Figure 5. $^1\text{H-NMR}$ spectrum of the solutions in the cathode (A) and anode (B) compartments in a 2-electrode electrochemical configuration. Signals at 7.92, 3.01 and 2.98 ppm are the internal standard DMF, while the singlet at 8.44 ppm is formate. The concentration of formate in catholyte was $\sim 1 \text{ mM}$, and no formate was detected in the anolyte by $^1\text{H-NMR}$ spectroscopy. The membrane area was $\sim 0.03 \text{ cm}^2$, and the

membrane current density during operation was 8.5 mA cm^{-2} . The volumes of the catholyte and anolyte were 50 ml and 25 ml, respectively. The operation time was 3 hours. When the concentration of formate in the catholyte increased to 0.1 M, and the area of the BPM increased to 0.12 cm^2 (other conditions unchanged), a small amount of formate ($\sim 16 \text{ }\mu\text{M}$) in the anolyte was detected by $^1\text{H-NMR}$ spectrum (C) after 3 hours of operation. The current density for formate crossover from the catholyte to anolyte was $\sim 30 \text{ }\mu\text{A cm}^{-2}$.

Integration of cathode, anode and bipolar membrane

Figure 1 shows a schematic illustration of the two-electrode electrochemical setup. The geometric areas of the GaAs/InGaP/TiO₂/Ni photoanode, bipolar membrane, Nafion membrane, and Pd/C/Ti cathode were mutually similar, at 0.030 cm^2 , 0.030 cm^2 , 0.030 cm^2 and 0.040 cm^2 respectively. The relatively small active device area was due to the behavior of the photoanode in 1.0 M KOH(aq). Figure 6A shows the current density for the unassisted CO₂R reaction as a function of the time under 100 mW cm^{-2} of simulated AM1.5 illumination, when the GaAs/InGaP/TiO₂/Ni photoanode was directly wired to the Pd/C nanoparticle-coated Ti mesh cathode without application of any external bias. The photocurrent density was $8.7 \pm 0.5 \text{ mA cm}^{-2}$. The overpotential for the Pd/C nanoparticle-coated Ti mesh cathode was recorded during the 3 h stability test, as shown in Figure 6B. During the stability test, the overpotential was between -40 mV and -100 mV; therefore, as shown in Figure 2B, the Faradaic efficiency of CO₂ reduction to formate was $\sim 100\%$, 98%, 95%, 94% after 30 min, 1 h, 2 h, 3 h, respectively. The corresponding solar-to-formate conversion efficiency at these times was thus 10.5%, 10.3%, 10.0%, and 9.9%, respectively. The solar-to-fuels efficiency is defined by:

$$\eta_{STF} = \frac{1.21 \text{ V} \times I_{\text{electrode}} \text{ mA cm}^{-2} \times \text{Faradaic efficiency of formate}}{100 \text{ mW cm}^{-2}} \quad [1]$$

1.21 V is the voltage required for the full chemical reaction, $2\text{OH}^- + 2\text{CO}_2 = 2\text{HCOO}^- + \text{O}_2$; 100 mW cm^{-2} is the solar power intensity.

The photocurrent density vs voltage behavior of the 2-electrode system (Figure 6C) exhibited mutually similar onset potentials and light-limited current densities before and after a 3 h stability test (Figure 6A), indicating minimal corrosion of the photoanode over this time period.

Figure 7 shows the measured (red) and calculated (dotted black) 2-electrode current density vs voltage behavior of the GaAs/InGaP/TiO₂/Ni photoanode wired to a Pd/C-coated Ti mesh cathode under 100 mW cm^{-2} of simulated Air Mass (AM) 1.5 illumination. The calculated 2-electrode current density vs voltage behavior (dotted black) was obtained by using the current-voltage behavior of the tandem solid-state photoabsorber (dotted orange) in conjunction with the overall polarization characteristic of a p⁺-Si/TiO₂/Ni anode and a Pd/C-coated Ti mesh cathode in the 2-electrode BPM configuration (KHCO₃/BPM/KOH) (black). The calculated 2-electrode current density vs voltage behavior was in good agreement with the experimental measurements. The electrosynthetic cell component required 2.04 V to operate at a current density of 8.5 mA cm^{-2} , and was thus well matched to the maximum power point of the photovoltaic tandem junction component of in the photoanode. Figure 7 also shows the overall polarization characteristics of the 2-electrode Nafion membrane configuration (KHCO₃/Nafion/KHCO₃) (blue) using the same electrode materials. Due to the large overpotential for the Ni catalyst to effect the OER at the near-neutral pH (Figure 3), obtaining an operational current density of $\sim 8.5 \text{ mA cm}^{-2}$ to drive the overall CO₂R reaction in conjunction with the OER required an additional $\sim 180 \text{ mV}$ of voltage in the Nafion-containing cell relative

to the voltage required to operate the BPM-containing cell (consistent with the voltage data summarized in Table I). Transport of K^+ between the anolyte and catholyte during steady-state operation would also electro-dialyze the electrolytes in the Nafion-containing cell. Circulation or recirculation might potentially minimize the steady-state K^+ -ion concentration polarization of the system,(22) but would entail significant challenges in separation of the low concentration of the liquid product, formate, in the catholyte. In contrast, the robust product separation afforded by the BPM would allow for production of a high concentration of formate, which would be advantageous in a down-stream separation process. Additionally, the Ni catalyst is not stable for OER at near-neutral pH.(23) Use of the bipolar membrane thus relaxed the electrolyte constraints and allowed the incorporation of this active OER catalyst(24) in the device.

Table I. Comparison of voltage losses for three cell configurations at $J_{\text{electrode/membrane}} = 8.5 \text{ mA cm}^{-2}$

Components	(Cathode) 2.8 M $\text{KHCO}_3/\text{BPM}/1.0 \text{ M KOH}$ (Anode)	(Cathode) 2.8 M $\text{KHCO}_3/\text{BPM}/2.8 \text{ M KHCO}_3$ (Anode)	(Cathode) 2.8 M $\text{KHCO}_3/\text{Nafion Membrane}/2.8 \text{ M KHCO}_3$ (Anode)
Membrane	$\sim 0.48 \text{ V}$	$\sim 0.82 \text{ V}$ (Figure S8)	$\sim 0.18 \text{ V}$
Ni OER overpotential	$0.320 \pm 0.007 \text{ V}$	$0.783 \pm 0.026 \text{ V}$	$0.783 \pm 0.026 \text{ V}$
Pd/C coated Ti mesh CO_2R to formate overpotential	$0.052 \pm 0.008 \text{ V}$	$0.052 \pm 0.008 \text{ V}$	$0.052 \pm 0.008 \text{ V}$
Total voltage loss	$\sim 0.85 \text{ V}$	$\sim 1.66 \text{ V}$	$\sim 1.01 \text{ V}$

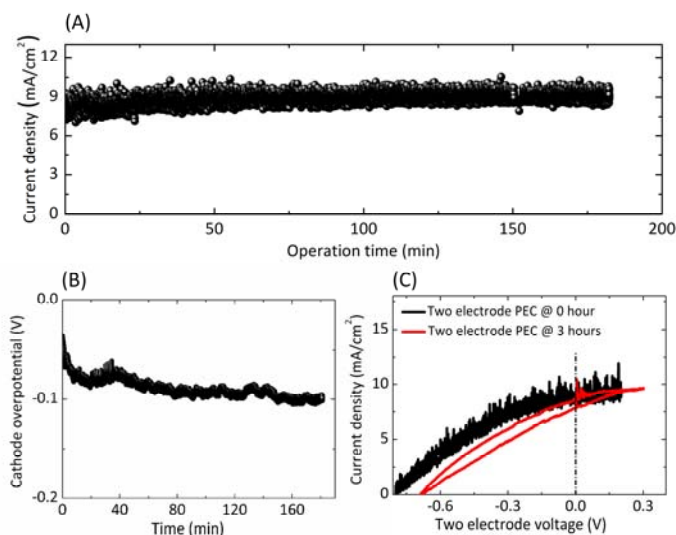


Figure 6. (A) The unassisted CO_2R current density as a function of operational time using a GaAs/InGaP/TiO₂/Ni photoanode and a Pd/C-coated Ti mesh cathode in a 2-electrode electrochemical configuration (Figure 3A) under 100 mW cm^{-2} of simulated AM1.5 illumination. (B) The overpotential for a Pd/C cathode during solar-driven CO_2R using GaAs/InGaP/TiO₂/Ni as a photoanode in a 2-electrode electrochemical configuration under simulated AM1.5 1-Sun illumination. (C) 2-electrode J - V behavior with a GaAs/InGaP/TiO₂/Ni photoanode and a Pd/C on Ti mesh cathode in a BPM configuration under simulated AM1.5 1-Sun illumination at 0 and 3 h, respectively, of the stability test.

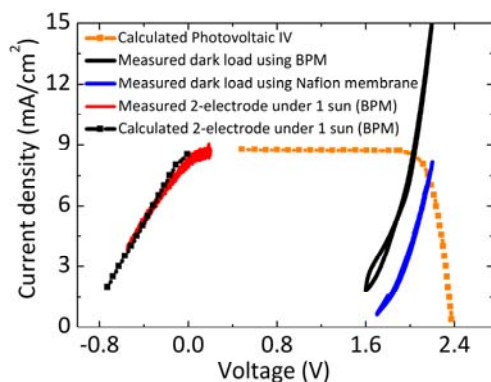


Figure 7. The overall polarization characteristics for the CO₂R reaction and the OER using a p⁺-Si/TiO₂/Ni anode and a Pd/C-coated Ti mesh cathode in the 2-electrode BPM configuration (KHCO₃/Nafion/KOH) (black) as well as in the 2-electrode Nafion membrane configuration (KHCO₃/Nafion/ KHCO₃) (blue). The measured (red) and calculated (black) 2-electrode current-voltage behavior of the GaAs/InGaP/TiO₂/Ni photoanode wired to a Pd/C-coated Ti mesh cathode were measured under 100 mW cm⁻² of simulated AM1.5 illumination. The calculated current density-voltage characteristic of the solid-state tandem cell (orange)(18, 19).

Conclusion

In summary, a solar-driven CO₂ reduction photovoltaic-assisted electrochemical cell was demonstrated at a solar-to-fuels energy-conversion efficiency of 10% using a tandem GaAs/InGaP/TiO₂/NiO_x photoanode in 1.0 M KOH(aq), a Pd/C nanoparticle coated Ti mesh cathode in 2.8 M KHCO₃(aq), and a bipolar membrane reducing a purified feed stream of 1 atm CO₂(g). At the operational current density of 8.5 mA cm⁻², the cathode exhibited <100 mV overpotential and >94% Faradaic efficiency for CO₂ reduction to formate in 2.8 M KHCO₃(aq) (pH=8.0), the anode exhibited 320 ± 7 mV overpotential for OER in 1.0 M KOH (aq) (pH=13.7), and the bipolar membrane exhibited ~480 mV voltage loss with minimal product crossovers and >90% and >95% selectivity for proton and hydroxide ions, respectively. The bipolar membrane effectively coupled together two electrolytes that were separately effective for the CO₂R reaction and for the OER, and produced lower total overpotentials and higher efficiency than could at present be obtained in a single-electrolyte CO₂ reduction cell.

Acknowledgments

This material is based upon work performed by the Joint Center for Artificial Photosynthesis, a DOE Energy Innovation Hub, supported through the Office of Science of the U.S. Department of Energy under Award Number DE-SC0004993. S.A.F. acknowledges the Resnick Sustainability Institute at Caltech for a Postdoctoral Fellowship. The authors also thank N. Dalleska (Caltech) for his assistance with measurements and analysis of the ICPMS and TIC data.

References

1. N. S. Lewis, G. Crabtree, A. J. Nozik, M. R. Wasielewski, P. Alivisatos, H. Kung, J. Tsao, E. Chandler, W. Walukiewicz, M. Spitler, R. Ellingson, R. Overend, J. Mazer, M. Gress, J. Horwitz, C. Ashton, B. Herndon, L. Shapard and R. M. Nault, Basic Research Needs for Solar Energy Utilization. Report of the Basic Energy Sciences Workshop on Solar Energy Utilization, in, p. Medium: ED, Office of Science, U. S. Department of Energy, Washington, DC (2005).
2. N. S. Lewis, *Science*, **351**, aad1920 (2016).
3. N. Gupta, M. Gattrell and B. MacDougall, *J. Appl. Electrochem.*, **36**, 161 (2006).
4. M. R. Singh, E. L. Clark and A. T. Bell, *Phys. Chem. Chem. Phys.*, **17**, 18924 (2015).
5. Y. Chen, N. S. Lewis and C. Xiang, *Energy Environ. Sci.*, **8**, 3663 (2015).
6. B. Kumar, M. Llorente, J. Froehlich, T. Dang, A. Sathrum and C. P. Kubiak, *Annu Rev Phys Chem*, **63**, 541 (2012).
7. Y. Hori, H. Wakebe, T. Tsukamoto and O. Koga, *Electrochim Acta*, **39**, 1833 (1994).
8. X. Min and M. W. Kanan, *J. Am. Chem. Soc.*, **137**, 4701 (2015).
9. M. Schreier, L. Curvat, F. Giordano, L. Steier, A. Abate, S. M. Zakeeruddin, J. Luo, M. T. Mayer and M. Gratzel, *Nat. Commun.*, **6**, 7326 (2015).
10. M. Asadi, B. Kumar, A. Behranginia, B. A. Rosen, A. Baskin, N. Reppin, D. Pisasale, P. Phillips, W. Zhu, R. Haasch, R. F. Klie, P. Král, J. Abiade and A. Salehi-Khojin, *Nat. Commun.*, **5**, 4470 (2014).
11. M. Asadi, K. Kim, C. Liu, A. V. Addepalli, P. Abbasi, P. Yasaei, P. Phillips, A. Behranginia, J. M. Cerrato, R. Haasch, P. Zapol, B. Kumar, R. F. Klie, J. Abiade, L. A. Curtiss and A. Salehi-Khojin, *Science*, **353**, 467 (2016).
12. B. Zhang, X. L. Zheng, O. Voznyy, R. Comin, M. Bajdich, M. Garcia-Melchor, L. L. Han, J. X. Xu, M. Liu, L. R. Zheng, F. P. G. de Arquer, C. T. Dinh, F. J. Fan, M. J. Yuan, E. Yassitepe, N. Chen, T. Regier, P. F. Liu, Y. H. Li, P. De Luna, A. Janmohamed, H. L. L. Xin, H. G. Yang, A. Vojvodic and E. H. Sargent, *Science*, **352**, 333 (2016).
13. C. C. L. McCrory, S. H. Jung, J. C. Peters and T. F. Jaramillo, *J. Am. Chem. Soc.*, **135**, 16977 (2013).
14. C. C. L. McCrory, S. Jung, I. M. Ferrer, S. M. Chatman, J. C. Peters and T. F. Jaramillo, *J. Am. Chem. Soc.*, **137**, 4347 (2015).
15. J. O. M. Bockris, A. K. Reddy and M. E. Gamboa-Aldeco, *Modern Electrochemistry*, Springer, New York City, U.S.A. (2000).
16. C. Xiang, K. M. Papadantonakis and N. S. Lewis, *Mater. Horiz.*, **3**, 169 (2016).
17. X. Zhou, R. Liu, K. Sun, Y. Chen, E. Verlage, S. A. Francis, N. S. Lewis and C. Xiang, *ACS Energy Letters*, **1**, 764 (2016).
18. K. Sun, R. Liu, Y. Chen, E. Verlage, N. S. Lewis and C. Xiang, *Adv. Energy Mater.*, **6**, 1600379 (2016).
19. E. Verlage, S. Hu, R. Liu, R. J. R. Jones, K. Sun, C. Xiang, N. S. Lewis and H. A. Atwater, *Energy Environ. Sci.*, **8**, 3166 (2015).
20. R. Kortlever, I. Peters, S. Koper and M. T. M. Koper, *ACS Catal.*, **5**, 3916 (2015).
21. K. Sun, F. H. Saadi, M. F. Lichterman, W. G. Hale, H.-P. Wang, X. Zhou, N. T. Plymale, S. T. Omelchenko, J.-H. He, K. M. Papadantonakis, B. S. Brunschwig and N. S. Lewis, *Proc. Natl. Acad. Sci. U.S.A.*, **112**, 3612 (2015).

22. M. A. Modestino, K. A. Walczak, A. Berger, C. M. Evans, S. Haussener, C. Koval, J. S. Newman, J. W. Ager and R. A. Segalman, *Energy Environ. Sci.*, **7**, 297 (2014).
23. A. Minguzzi, F.-R. F. Fan, A. Vertova, S. Rondinini and A. J. Bard, *Chem. Sci.*, **3**, 217 (2012).
24. L. Trotochaud, S. L. Young, J. K. Ranney and S. W. Boettcher, *J. Am. Chem. Soc.*, **136**, 6744 (2014).